ISSN 0021-3640, JETP Letters, 2020, Vol. 112, No. 9, pp. 568–576. © Pleiades Publishing, Inc., 2020.

CONDENSED MATTER

Investigation Insights into Electronic Structures, Exchange Splittings, Induced Ferromagnetism, and Half-Metallic Feature in New Ti-Doped BaS

B. Doumi[a, b, *], A. Mokaddem[b, c, **], and A. Tadjer[d]

[a] *Faculty of Sciences, Department of Physics, Dr. Tahar Moulay University of Saida, Saida, 20000 Algeria*
[b] *Instrumentation and Advanced Materials Laboratory, University Center of Nour Bachir El-Bayadh, El-Bayadh, 32000 Algeria*
[c] *University Center of Nour Bachir El-Bayadh, El-Bayadh, 32000 Algeria*
[d] *Modelling and Simulation in Materials Science Laboratory, Physics Department, Djillali Liabes University of Sidi Bel-Abbes, Sidi Bel-Abbes, 22000 Algeria*
**e-mail: bdoummi@yahoo.fr*
***e-mail: mokaddem.allel@gmail.com*

Received September 19, 2020; revised September 27, 2020; accepted September 27, 2020

The new $Ba_{1-x}Ti_xS$ compounds based on the titanium (Ti)-doped BaS at various concentrations $x = 0.25$, 0.5, and 0.75 were characterized using the first-principle concepts of density functional theory. We investigated the doping effect of titanium on the structural and electronic properties, induced ferromagnetism, half-metallicity, and exchange splittings in $Ba_{1-x}Ti_xS$ materials. The origin of ferromagnetism in the $Ba_{1-x}Ti_xS$ compounds is due to the localized partially occupied 3*d* (Ti) states related to the double exchange mechanism. The electronic structures of $Ba_{1-x}Ti_xS$ at concentrations $x = 0.25$ and 0.5 show half-metallic ferromagnetic character with spin polarization of 100%. For the concentration $x = 0.75$, the $Ba_{0.25}Ti_{0.75}S$ compound exhibits a metallic nature for two spins channels due to widening 3d (Ti) states in the gap. Therefore, $Ba_{1-x}Ti_xS$ at concentrations $x = 0.25$ and 0.5 seems to be a candidate for spintronics.

DOI: 10.1134/S0021364020210018

1. INTRODUCTION

The progress of electronic device technology requires reducing the size of electronic components and increasing the speed of data processing. In this respect, a modern field of electronics known as spin-based electronics or spintronics [1, 2] has been developed, where the spin of electron is exploited as a second advantage in addition to its charge aspect in order to create new functionalities in innovative spin-based devices [3–5]. The dilute magnetic semiconductors (DMS) have been studied extensively due to their electronic and magnetic performances, which have considerable interest for various applications in new spintronics devices [6–11]. The advanced technologies of spintronic devices such as magnetic sensors, giant and tunnel magnetoresistance are based on half-metallic (HM) ferromagnetic materials [12–16]. The emergence of the half-metallic ferromagnetic character in DMS allows to benefit from both magnetic and semiconductor properties [6, 17, 18], which make them ideal materials for spintronics where the two properties of the electron, spin and charge, are utilized to achieve a multifunction variety [19, 20].

The barium chalcogenides BaS, BaSe, and BaTe are binary compounds of the alkaline earth type, where they crystallize in the NaCl (B1) structure under normal conditions and undergo a phase transition to the CsCl type phase (B2) under pressure [21–25]. These materials are characterized by indirect wide band-gap semiconductors and their important technological applications in optoelectronics such as laser diodes in blue-light wavelength region and light-emitting diodes [26]. The electronic and half-metallic ferromagnetic properties of DMS based on transition metal-doped BaS, BaSe, and BaTe compounds have been the subject of several first-principle theoretical studies in order to predict their use for possible spintronics applications [27–29]. According to these works, the DMS compounds obtained from magnetic impurities at low concentrations such as BaS doped with vanadium (V) [27], the BaTe doped with chromium (Cr) [28] and the BaS doped with Cr [29] are promising materials for future spintronics applications.

Author's ORCID ID: http://orcid.org/0000-0003-1563-8587

Table 1. Computed lattice constants (a), bulk moduli (B) and their pressure derivatives (B') for BaS, $Ba_{0.75}Ti_{0.25}S$, $Ba_{0.5}Ti_{0.5}S$, and $Ba_{0.25}Ti_{0.75}S$ other experimental data and theoretical calculations

Compound	a, Å	B, GPa	B'	GGA-WC method
Our calculations				
BaS	6.348	46.73	4.47	
$Ba_{0.75}Ti_{0.25}S$	6.102	50.79	4.51	
$Ba_{0.5}Ti_{0.5}S$	5.825	55.79	3.67	
$Ba_{0.25}Ti_{0.75}S$	5.364	66.12	5.94	
Other calculations				
BaS	6.387 ± 0.002 [21]	55.1 [39]	5.5 [39]	Experimental
	6.372 [27]	46.21 [27]	4.66 [27]	GGA-WC
	6.343 [41]	44.51 [41]	4.205 [41]	GGA-WC
	6.343 [42]	38.35 [42]	4.205 [42]	GGA-WC
	6.343 [43]	44.399 [43]	4.167 [43]	GGA-WC
	6.335 [44]	45.725 [44]		GGA-WC
	6.41 [40]	47.32 [40]	4.75 [40]	GGA-PBE
	6.435 [44]	40.8031 [44]		GGA-PBE
	6.274 [44]	51.0230 [44]		LDA

In this study, we have studied the electronic structures, induced ferromagnetism, half-metallic property and exchange splittings in titanium (Ti)-doped BaS such as $Ba_{1-x}Ti_xS$ materials under the effect of doping with Ti impurities at concentrations $x = 0.25$, 0.5, and 0.75. The calculations were performed using the ab initio methods of density functional theory [30, 31].

2. COMPUTATIONAL METHOD AND DETAILS OF CALCULATIONS

We have utilized the WIEN2K package [32] based on the computational ab initio approaches of DFT [30, 31] and full-potential linearized augmented plane-wave (FP-LAPW) [33] to study the structural, electronic, and magnetic properties of $Ba_{1-x}Ti_xS$ at various concentrations $x = 0.25$, 0.5, and 0.75. Under normal conditions, the BaS adopts the rock-salt NaCl (B1) type structure with space group no. 225 $Fm\bar{3}m$. In the conventional structure of BaS, the Ba and S atoms are located at the (0, 0, 0) and (0.5, 0.5, 0.5) sites, respectively. We have substituted the Ba_4S_4 supercells by one, two and Ti atoms at the Ba sites to generate respectively the Ba_3TiS_4, $Ba_2Ti_2S_4$, and $BaTi_3S_4$ supercells equivalent to $Ba_{0.75}Ti_{0.25}S$ for concentration $x = 0.25$, $Ba_{0.5}Ti_{0.5}S$ for $x = 0.5$ and $Ba_{0.25}Ti_{0.75}S$ for $x = 0.75$. The $Ba_{0.5}Ti_{0.5}S$ owns tetragonal structure with space group no. 123 $P4/mmm$, whilst the $Ba_{0.75}Ti_{0.25}S$ and $Ba_{0.25}Ti_{0.75}S$ have cubic structures space group no. 221 $Pm\bar{3}m$.

The generalized gradient approximation proposed by Wu and Cohen (GGA-WC) [34] is employed to calculate structural parameters of $Ba_{1-x}Ti_xS$ materials, while the Tran–Blaha modified Becke–Johnson (TB-mBJ) potential [35, 36] is used to obtain magnetic properties, exchange splittings, and perfect electronic structures with improved gaps. We have selected the mean radii of Muffin-tin spheres for Ba, S, and Ti atoms to ensure that the spheres do not overlap. The valence and core states are separated by a cutoff of −6 Ry. The wavefunctions have developed to plane waves by means of a cutoff $K_{max} = 9.0/R_{MT}$ at the interstitial sites, where the R_{MT} corresponds to the average radius of the muffin-tin sphere and K_{max} describes the size of the largest K vector in the plane wave. The charge density is extended in Fourier up to $G_{max} = 14$ (au)$^{-1}$, where G_{max} describes the largest vector in the Fourier expansion. The Brillouin zone sampling is performed with the Monkhorst–Pack mesh [37] by the use of (4 × 4 × 4) special k-points for $Ba_{0.75}Ti_{0.25}S$ and $Ba_{0.25}Ti_{0.75}S$, (4 × 4 × 3) for $Ba_{0.5}Ti_{0.5}S$ and (10 × 10 × 10) for BaS. The self-consistent is reached when the total energy converges towards 0.1 mRy.

3. RESULTS AND DISCUSSIONS

3.1. Structural Properties

We performed the optimization of structures by varying of total energies as a function of the volumes of supercells of $Ba_{1-x}Ti_xS$ systems. These variations were adjusted by the Murnaghan equation of state [38] to determine the equilibrium structural parameters of BaS, $Ba_{0.75}Ti_{0.25}S$, $Ba_{0.5}Ti_{0.5}S$, and $Ba_{0.25}Ti_{0.75}S$ materi-

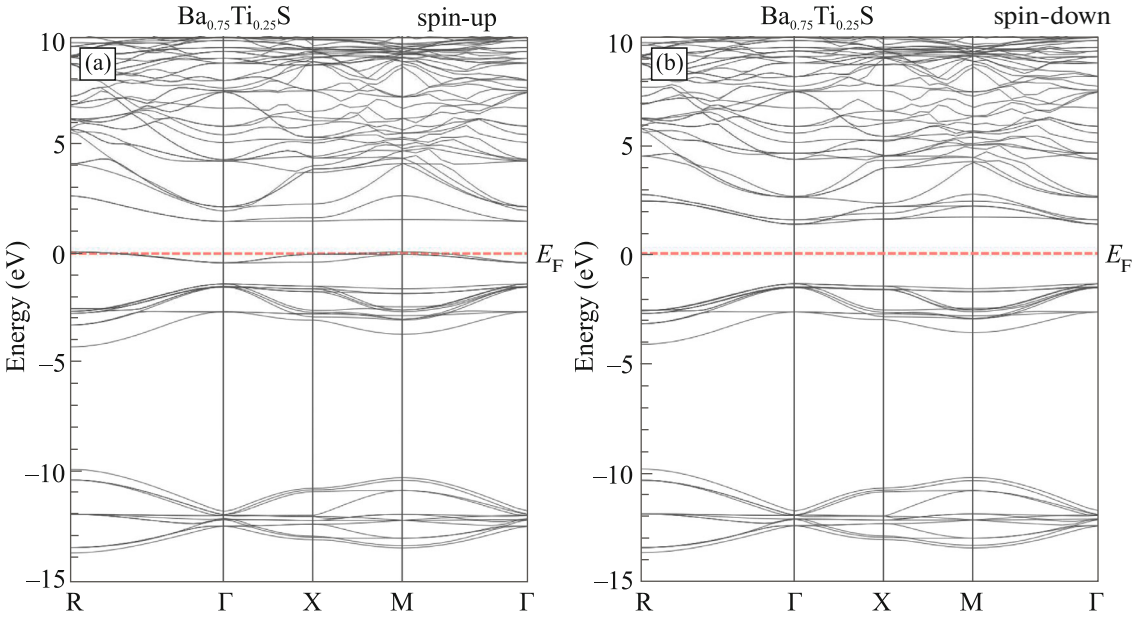

Fig. 1. (Color online) Spin-polarized band structures of $Ba_{0.75}Ti_{0.25}S$ for (a) majority spins (up) and (b) minority spins (down).

als. The results for lattice constants, bulk moduli (B) and their pressure derivatives (B') are given in Table 1. For comparison purposes, we have also presented with our results other experimental data [21, 39] and theoretical calculations [27, 40–44] obtained by GGA-WC [34], local density approximation (LDA) [45], and generalized gradient approximation of Perdew–Burke–Ernzerhof (GGA-PBE) [46]. The calculated lattice parameter and bulk modulus of BaS are consistent with experimental values [21, 39], theoretical GGA-WC calculations, and with GGA-PBE approximations. The better performance of the GGA-WC approximation for characterizing structural parameters is due to the fourth order expansion of its gradient of exchange and correlation functional [34]. On the other hand, the difference between the sizes of ionic radii of the Ba atom and the substituted Ti impurity causes variation of the lattice parameter. As a result, the bulk modulus increases when the lattice parameter decreases with raising the Ti concentration, leading to the hardness of $Ba_{1-x}Ti_xS$ ternary systems compared to the BaS binary compound.

3.2. Spin-Polarized Electronic Structures and Half-Metallic Properties

We consider in this section the electronic structures as well as the half-metallic behavior of $Ba_{1-x}Ti_xS$ materials at concentrations $x = 0.25$, 0.5, and 0.75. The calculations of the electronic properties were performed using the TB-mBJ potential [35, 36], which improves the band structures and gives perfect values for the gaps. Figures 1–3 show the computed spin-polarized band structures of $Ba_{0.75}Ti_{0.25}S$, $Ba_{0.5}Ti_{0.5}S$, and $Ba_{0.25}Ti_{0.75}S$, respectively. For the two concentrations $x = 0.25$ and 0.5, the $Ba_{0.75}Ti_{0.25}S$, $Ba_{0.5}Ti_{0.5}S$ compounds reveal a half-metallic ferromagnetic behavior resulted from metallic nature of majority-spin bands and semiconducting minority-spin bands. In contrast, the $Ba_{0.25}Ti_{0.75}S$ at high concentration $x = 0.75$ has metallic character because the Fermi level E_F is dominated by bands for both majority-spin and minority-spin directions. The semiconductor minority spins of both $Ba_{0.75}Ti_{0.25}S$, $Ba_{0.5}Ti_{0.5}S$ materials are characterized by the half-metallic ferromagnetic gap, which corresponds to the separation between the maximum of the valence band and the minimum of the conduction band. Another gap used for characterizing minority spins is known as half-metallic gap; it determines the smallest energy between the absolute value of energy of valence band maximum for majority (minority)-spin and the energy of the conduction band minimum for majority (minority)-spin with respect to the Fermi level [47, 48].

The computed half-metallic ferromagnetic gaps (G_{HMF}) and half-metallic gaps (G_{HM}) are summarized in Table 2. The metallic character of the $Ba_{1-x}Ti_xS$ compounds is due to the localized 3d states of titanium (Ti) in the gap that overlap with Fermi level. In the case of both $Ba_{0.75}Ti_{0.25}S$, $Ba_{0.5}Ti_{0.5}S$ materials, the 3d (Ti) levels are located at the bottom of conduction bands of minority spins far than Fermi level. The $Ba_{0.75}Ti_{0.25}S$ compound has a large half-metallic (HM) gap of 1.35 eV, which represents the absolute value of energy of valence band maximum for minority-spin bands with respect to the Fermi level. For concentra-

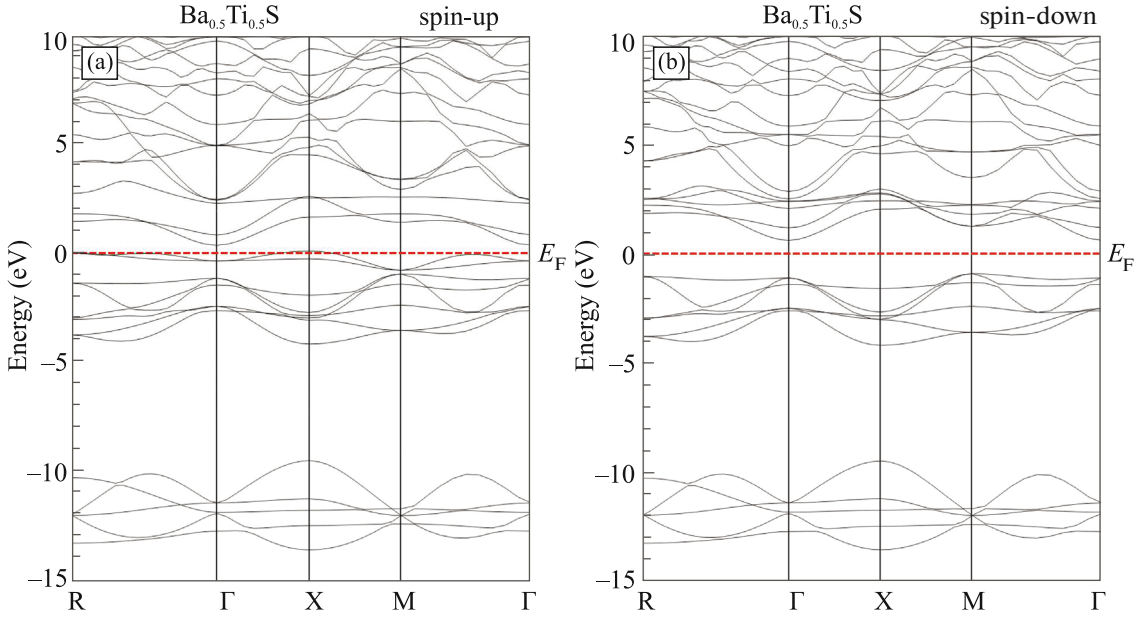

Fig. 2. (Color online) Spin-polarized band structures of $Ba_{0.5}Ti_{0.5}S$ for (a) majority spins (up) and (b) minority spins (down).

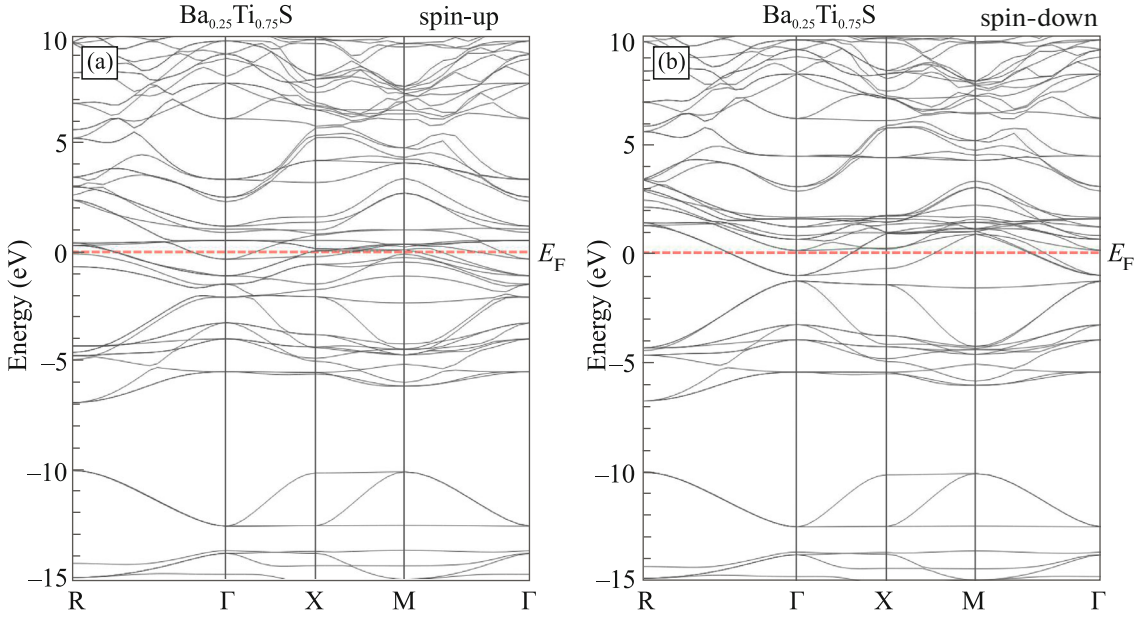

Fig. 3. (Color online) Spin-polarized band structures of $Ba_{0.25}Ti_{0.75}S$ for (a) majority spins (up) and (b) minority spins (down).

tion $x = 0.5$, the $3d$ (Ti) levels positioned at the bottom of conduction bands of minority spins moves towards Fermi level due to increase in concentration of (Ti), leading to the shift of HM gap above Fermi level. In this case, the HM gap of the $Ba_{0.5}Ti_{0.5}S$ equals to 0.51 eV, which corresponds to the energy of the conduction band minimum of minority-spin bands with respect to the Fermi level. For the high concentration $x = 0.75$, the $3d$ levels of the minority spins broaden strongly in the gap, where their states dominate Fermi level. Thus, the $Ba_{0.25}Ti_{0.75}S$ exhibits metallic nature for two spins channels.

The total and partial densities of states for $Ba_{0.75}Ti_{0.25}S$, $Ba_{0.5}Ti_{0.5}S$, and $Ba_{0.25}Ti_{0.75}S$ materials are given by Figs. 4–6. The contributions of total densities of states of majority and minority spins around Fermi level determine the polarization of spin-polarized

Table 2. Computed half-metallic ferromagnetic (HMF) gap (G_{HMF}) and half-metallic (HM) gap (G_{HM}) of minority-spin bands for $Ba_{0.75}Ti_{0.25}S$, $Ba_{0.5}Ti_{0.5}S$, and $Ba_{0.25}Ti_{0.75}S$

Compound	G_{HMF}, eV	G_{HM}, eV	$D\uparrow(E_F)$, states/eV	$D\downarrow(E_F)$, states/eV	P, %
$Ba_{0.75}Ti_{0.25}S$	2.73	1.35	1.346	0	100
$Ba_{0.5}Ti_{0.5}S$	1.73	0.51	0.1528	0	100
$Ba_{0.25}Ti_{0.75}S$	No G_{HMF}	No G_{HM}	4.646	1.591	48.98

material. The polarization (P) of each $Ba_{1-x}Ti_xS$ doping compound is given by the expression [49]

$$P = \frac{|D\uparrow(E_F) - D\downarrow(E_F)|}{|D\uparrow(E_F) + D\downarrow(E_F)|}, \quad (1)$$

where $D\uparrow(E_F)$ and $D\downarrow(E_F)$ are the total densities of states (DOSs) for majority and minority spins at the Fermi level E_F, respectively. The values of DOS at E_F for both spin directions as well as the polarization (P) of $Ba_{1-x}Ti_xS$ compounds at different concentrations are given in Table 2. The non-zero values of $D\uparrow(E_F)$ and $D\downarrow(E_F)$ at the Fermi level for the high concentration $x = 0.75$ suggest that the $Ba_{0.25}Ti_{0.75}S$ is metallic in nature. For both $Ba_{0.75}Ti_{0.25}S$ and $Ba_{0.5}Ti_{0.5}S$ materials, the majority-spin states are metallic due to p–d hybridization between p (S) and $3d$ (Ti) levels around Fermi level, while the minority spins have no states at the Fermi level. Therefore, $D\uparrow(E_F)$ are not zero, whereas $D\downarrow(E_F)$ equals to zero, meaning that $P = 1$. Consequently, $Ba_{1-x}Ti_xS$ at concentrations $x = 0.25$ and 0.5 are half-metallic ferromagnetic with spin polarizations of 100% and appear to be good candidates for spintronics applications.

Moreover, Figs. 4a and 5a show that the upper part of valence bands for majority spins are dominated by the main contribution of Ti atoms and small contributions of Ba and S atoms. The valence bands for two spins directions are mainly populated by the p (S) states with minor contributions of p (Ba) and $3d$ (Ti) states in the range of −3.6 to −1.2, −4.6 to −1.3 eV for $Ba_{0.75}Ti_{0.25}S$ and $Ba_{0.5}Ti_{0.5}S$. In $Ba_{1-x}Ti_xS$ materials, the S ions create an octahedral crystal field around Ti site, which splits the five-fold degenerate $3d$ levels into three low-lying t_{2g} (d_{xy}, d_{xz}, and d_{yz}) and two high-lying e_g (d_{z^2} and $d_{x^2-y^2}$) symmetry states as shown in Figs. 4b, 5b, and 6b. The partial densities of states demonstrate that the e_g states are located at high energies compared to t_{2g} states, confirming that the Ti ion is positioned in the octahedral environment. The double-exchange model is used by Sato et al. [50, 51] to

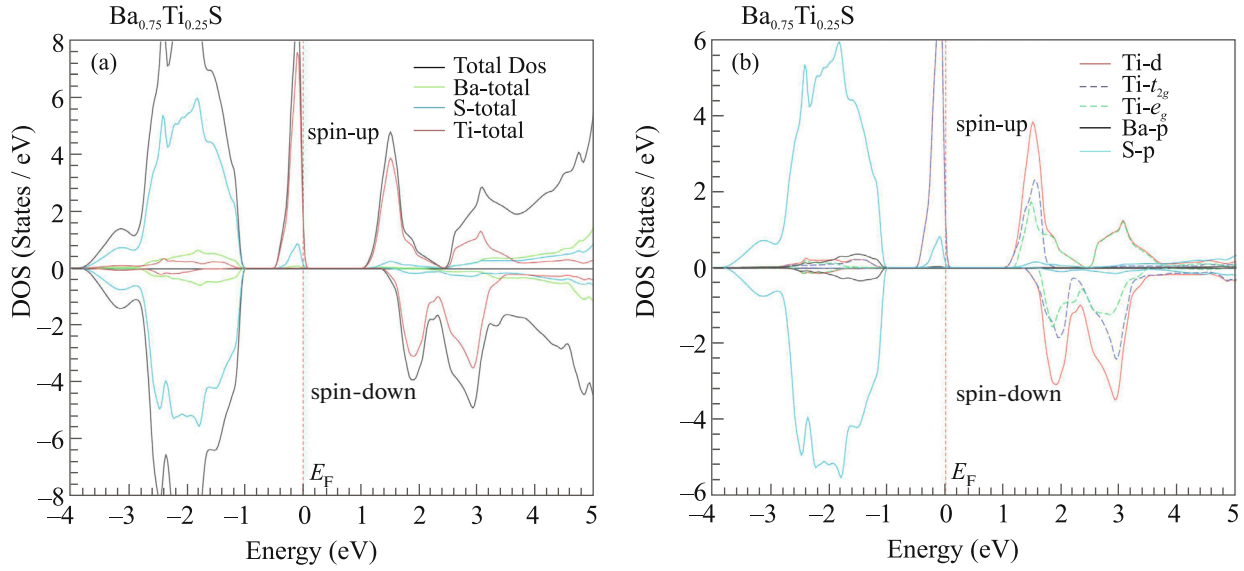

Fig. 4. (Color online) Spin-polarized total and partial densities of states (DOS) of $Ba_{0.75}Ti_{0.25}S$. (a) Total DOS of Ba, S, and Ti and (b) partial DOSs of d (Ti), t_{2g} (Ti), e_g (Ti), p (Ba), and p (S).

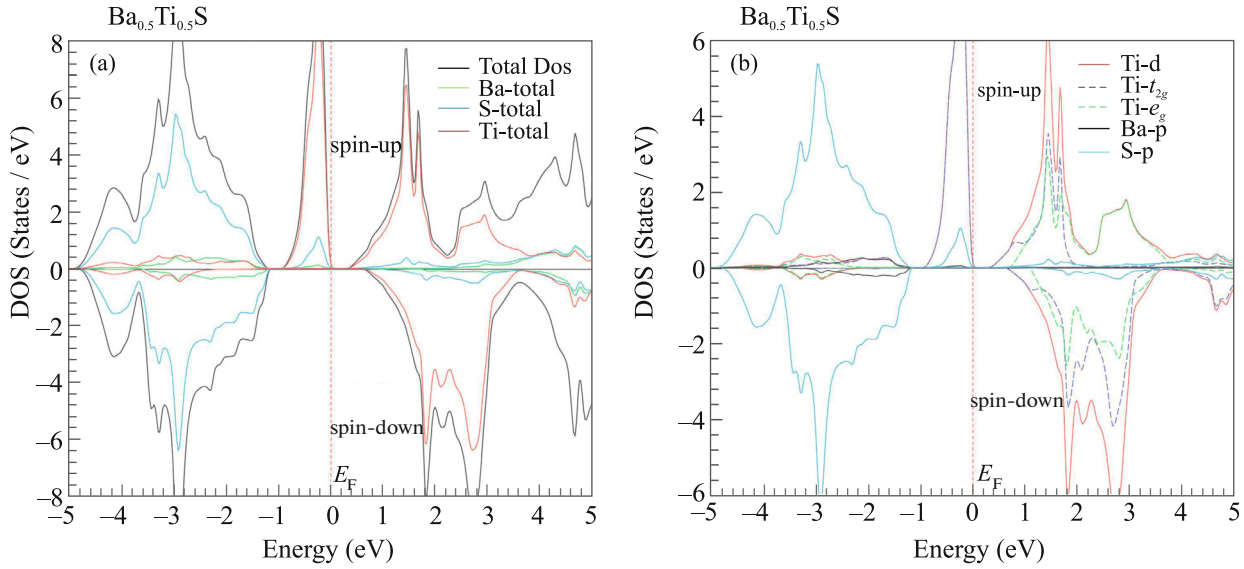

Fig. 5. (Color online) Spin-polarized total and partial densities of states (DOS) of $Ba_{0.5}Ti_{0.5}S$. (a) Total DOS of Ba, S, and Ti and (b) partial DOS of *d* (Ti), t_{2g} (Ti), e_g (Ti), *p* (Ba), and *p* (S).

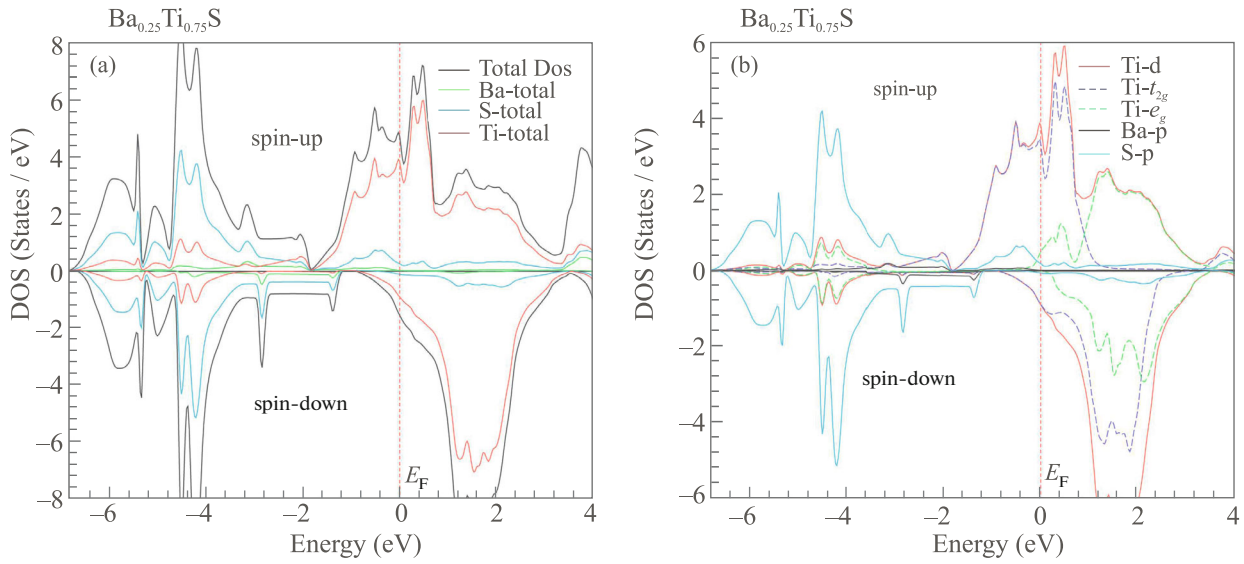

Fig. 6. (Color online) Spin-polarized total and partial densities of states (DOS) of $Ba_{0.25}Ti_{0.75}S$. (a) Total DOS of Ba, S, and Ti and (b) partial DOS of *d* (Ti), t_{2g} (Ti), e_g (Ti), *p* (Ba) and *p* (S).

elucidate the origin of magnetism in DMS doped with transition metals (TM) in which the 3*d* (TM) states are partially occupied. In $Ba_{1-x}Ti_xS$ materials, the 3*d* (Ti) levels are partially occupied because the e_g states are empty sited at the bottom of conduction bands and t_{2g} are partially occupied states. Consequently, 3*d* (Ti) partially filled states suggest the stability of ferromagnetic configuration in $Ba_{1-x}Ti_xS$ compounds associated with double exchange mechanism [52].

3.3. Magnetic Properties

3.3.1. Magnetic moments. In $Ba_{1-x}Ti_xS$ materials, the Ti magnetic impurity substituted at Ba site contributes two electrons to the *p* states of S ion and keeps two unpaired electrons in the 3*d* levels. Thus, the 3*d* (Ti) partially occupied states are localized at the Fermi level and create hole-type acceptor carriers, which produce magnetism in the $Ba_{1-x}Ti_xS$ compounds. The two unpaired electrons of the partially occupied 3*d*

(Ti) states induce a total magnetic moment of $2\mu_B$ per Ti ion, where μ_B is the Bohr magneton. Table 3 summarizes the calculated total and partial magnetic moments of relevant Ti, Ba, and S atoms and in interstitial sites for $Ba_{0.75}Ti_{0.25}S$, $Ba_{0.5}Ti_{0.5}S$, and $Ba_{0.25}Ti_{0.75}S$ compounds. The positive partial magnetic moments of Ti, Ba, and S for all $Ba_{1-x}Ti_xS$ materials reveal that the magnetic spins of Ti, Ba, and S interact ferromagnetically. For $Ba_{0.75}Ti_{0.25}S$ and $Ba_{0.5}Ti_{0.5}S$ compounds, the magnetic moments of Ti atoms are reduced less than 2 and 4 μ_B as well as weak moments result on the Ba and S sites due to the p–d exchange interaction between p (S) and $3d$ (Ti) states.

3.3.2. Exchange constants and exchange splittings. The exchange couplings between the substituted magnetic Ti impurity and the conduction and valence states are described by the two parameters $N_0\alpha$ and $N_0\beta$ known as the exchange constants. The parameter $N_0\alpha$ corresponds to the exchange coupling between the s-type conduction bands and $3d$ (Ti) levels, whereas the exchange coupling between the p-type valence bands and $3d$ (Ti) levels is characterized by the constant $N_0\beta$. These two parameters are determined by the mean-field theory using the expressions [53, 54]

$$N_0\alpha = \frac{\Delta E_c}{x\langle s\rangle}, \quad (2)$$

$$N_0\beta = \frac{\Delta E_v}{x\langle s\rangle}, \quad (3)$$

where $\Delta E_c = E_c^{\downarrow} - E_c^{\uparrow}$ and $\Delta E_v = E_v^{\downarrow} - E_v^{\uparrow}$ represent the difference energies at the high symmetry point Γ respectively of the conduction and valence band-edge spin-splittings. The quantities $\langle s\rangle$ and x correspond to half the total magnetic moment per Ti ion and the concentration of Ti, respectively [53]. The calculated exchange parameters $N_0\alpha$ and $N_0\beta$ are presented in Table 4. The parameter $N_0\beta$ is negative for $Ba_{0.75}Ti_{0.25}S$ and $Ba_{0.5}Ti_{0.5}S$, indicating antiferromagnetic coupling between p-type valence bands and $3d$ (Ti) states. The parameter $N_0\alpha$ is negative and positive for concentrations $x = 0.25$ and 0.5, respectively, demonstrating that the exchange couplings between $3d$ (Ti) levels and s-type conduction bands are antiferromagnetic and ferromagnetic for $Ba_{0.75}Ti_{0.25}S$ and $Ba_{0.5}Ti_{0.5}S$, respectively.

In the $Ba_{1-x}Ti_xS$ materials, the e_g states are empty, while the t_{2g} partially occupied states creates one acceptor hole type carrier and hybridize with the host valence band. Therefore, the localized electrons of $3d$ (Ti) states at the top of valence bands generate ferromagnetism mediated by holes [55, 56]. The $\Delta_x(pd) = E_v^{\downarrow} - E_v^{\uparrow}$ indirect exchange splitting is important parameter to describe the magnitude of ferromagnetism in spin-polarized materials. It is determined from the difference between $E_v^{\downarrow}$ and $E_v^{\uparrow}$ energies of valence band maximums respectively for minority-spin and majority-spin bands. The calculated indirect exchange splittings of $Ba_{0.75}Ti_{0.25}S$ and $Ba_{0.5}Ti_{0.5}S$ compounds are given in Table 4. The values for $Ba_{0.75}Ti_{0.25}S$ and $Ba_{0.5}Ti_{0.5}S$ materials are negative because the valence band maximums of majority spins overlap with the Fermi level, while the valence band maximums of the minority spins are located at lower energies below Fermi level. This process results in a more attractive (negative) potential for the minority spins compared to the majority spins [57], generating strongly localized electronic states that endorse the ferromagnetic state in the $Ba_{0.75}Ti_{0.25}S$ and $Ba_{0.5}Ti_{0.5}S$ materials.

Table 3. Computed total and partial magnetic moments (in Bohr magneton μ_B) of relevant Ti, Ba, and S muffin-tin spheres and in the interstitial sites for $Ba_{0.75}Ti_{0.25}S$, $Ba_{0.5}Ti_{0.5}S$, and $Ba_{0.25}Ti_{0.75}S$

Magnetic moment per atom	$Ba_{0.75}Ti_{0.25}S$	$Ba_{0.5}Ti_{0.5}S$	$Ba_{0.25}Ti_{0.75}S$
Cr number 1 (μ_B)	1.7409	1.7125	1.3586
Cr number 2 (μ_B)	No atom	1.7125	1.3006
Cr number 3 (μ_B)	No atom	No atom	1.2785
Ba number 2 (μ_B)	0.0003	No atom	No atom
Ba number 3 (μ_B)	0.0018	0.0057	No atom
Ba number 4 (μ_B)	0.0018	0.0057	0.0199
S number 5 (μ_B)	0.0001	0.0138	0.0440
S number 6 (μ_B)	0.0114	0.0138	0.0475
S number 7 (μ_B)	0.0046	0.0115	0.0531
S number 8 (μ_B)	0.0046	0.0115	0.0083
Interstitial (μ_B)	0.2346	0.5132	0.8181
Total (μ_B)	2.0001	4.0002	4.9286

Table 4. Computed exchange couplings $N_0\alpha$ and $N_0\beta$ and indirect exchange splittings $\Delta_x(pd)$ of $Ba_{0.75}Ti_{0.25}S$ and $Ba_{0.5}Ti_{0.5}S$

Compound	$N_0\alpha$	$N_0\beta$	$\Delta_x(pd)$, eV
$Ba_{0.75}Ti_{0.25}S$	−0.273	−1.940	−1.347
$Ba_{0.5}Ti_{0.5}S$	0.216	−0.791	−1.221

4. CONCLUSIONS

The structural parameters, electronic structures, half-metallicity, ferromagnetic properties and exchange splittings in the $Ba_{1-x}Ti_xS$ compounds at different concentrations $x = 0.25$, 0.5, and 0.75 were

investigated by the use of the first-principle computations of DFT. The results of structural parameters of BaS are consistent with the experimental data and recent theoretical calculations due to better performance of GGA-WC functional for characterizing structural properties. The difference between the size of Ba and Ti ionic radii leads to the decrease in lattice parameter and increase in bulk modulus, and hence the $Ba_{1-x}Ti_xS$ compounds become harder than BaS. The calculations of electronic and magnetic properties with TB-mBJ potential allowed us to find that $Ba_{0.25}Ti_{0.75}S$ is metallic in nature, while the $Ba_{0.75}Ti_{0.25}S$ and $Ba_{0.5}Ti_{0.5}S$ compounds are half-metallic ferromagnetic with 100% spin polarizations. In $Ba_{0.75}Ti_{0.25}S$ and $Ba_{0.5}Ti_{0.5}S$, the ferromagnetic configuration is stabilized by 3*d* (Ti) partially occupied states associated with double exchange. The negative values of indirect exchange splittings suggest that the minority spins have attractive potential, which endorses the ferromagnetic state in the $Ba_{0.75}Ti_{0.25}S$ and $Ba_{0.5}Ti_{0.5}S$ compounds. In addition, the $Ba_{0.75}Ti_{0.25}S$ at weak concentration $x = 0.25$ exhibits large half-metallic gap than that of $Ba_{0.5}Ti_{0.5}S$. Consequently, $Ba_{1-x}Ti_xS$ materials doped with titanium at low concentration appear to be useful candidates for spin-injection in semiconductors spintronics.

REFERENCES

1. S. Wolf, D. Awschalom, R. Buhrman, J. Daughton, V. S. von Molnar, M. Roukes, A. Y. Chtchelkanova, and D. Treger, Science (Washington, DC, U. S.) **294**, 1488 (2001).
2. I. Žutić, J. Fabian, and S. D. Sarma, Rev. Mod. Phys. **76**, 323 (2004).
3. M. G. Kostenko, A. V. Lukoyanov, and E. I. Shreder, JETP Lett. **107**, 126 (2018).
4. S. Benatmane and S. Cherid, JETP Lett. **111**, 694 (2020).
5. S. D. Borisova, G. G. Rusina, S. Eremeev, and E. V. Chulkov, JETP Lett. **110**, 211 (2019).
6. S. Ghosal, H. Luitel, S. K. Mandal, D. Sanyal, and D. Jana, J. Phys. Chem. Solids **136**, 109175 (2020).
7. B. Doumi, A. Tadjer, F. Dahmane, A. Djedid, A. Yakoubi, Y. Barkat, M. O. Kada, A. Sayede, and L. Hamada, J. Supercond. Novel Magn. **27**, 293 (2014).
8. Santanu Das, A. Bandyopadhyay, Sukhen Das, and S. Sutradhar, J. Alloys Compd. **731**, 591 (2018).
9. H. Lakhdari, B. Doumi, A. Mokaddem, A. Sayede, J. P. Araújo, A. Tadjer, and M. Elkeurti, J. Supercond. Novel Magn. **32**, 1781 (2019).
10. L. Hua, J. Zhu, and Z. Lu, JETP Lett. **103**, 631 (2016).
11. E. Yakovleva, L. N. Oveshnikov, A. Kochura, K. Lisunov, E. Lahderanta, and B. A. Aronzon, JETP Lett. **101**, 130 (2015).
12. F. Estrada, E. Guzmán, O. Navarro, and M. Avignon, Phys. Rev. B **97**, 195155 (2018).
13. S. M. Thompson, J. Phys. D: Appl. Phys. **41**, 093001 (2008).
14. G. Binasch, P. Grünberg, F. Saurenbach, and W. Zinn, Phys. Rev. B **39**, 4828 (1989).
15. A. Fert, P. Grünberg, A. Barthélémy, F. Petroff, and W. Zinn, J. Magn. Magn. Mater. **140**, 1 (1995).
16. Q. Mahmood, M. Hassan, M. Yaseen, and A. Laref, Chem. Phys. Lett. **729**, 11 (2019).
17. I. Elahi, S. M. Alay-e-Abbas, S. Nazir, A. Shaukat, and M. N. Tahir, J. Magn. Magn. Mater. **477**, 249 (2019).
18. K. Korichi, B. Doumi, A. Mokaddem, A. Sayede, and A. Tadjer, Philos. Mag. **100**, 1172 (2020).
19. V. Y. Irkhin and M. I. Katsnel'son, Phys. Usp. **37**, 659 (1994).
20. M. S. Khan, L. Shi, B. Zou, and S. Ali, Comput. Mater. Sci. **174**, 109491 (2020).
21. S. Yamaoka, O. Shimomura, H. Nakazawa, and O. Fukunaga, Solid State Commun. **33**, 87 (1980).
22. S. T. Weir, Y. K. Vohra, and A. L. Ruoff, Phys. Rev. B **35**, 874 (1987).
23. T. A. Grzybowski and A. L. Ruoff, Phys. Rev. Lett. **53**, 489 (1984).
24. A. Ruoff and T. Grzybowski, *Solid State Physics under Pressure,* Ed. by S. Minomura (Terra Scientific, Tokyo, 1985).
25. T. Grzybowski and A. Ruoff, Phys. Rev. B **27**, 6502 (1983).
26. K. L. Heng, S. J. Chua, and P. Wu, Chem. Mater. **12**, 1648 (2000).
27. Z. Addadi, B. Doumi, A. Mokaddem, M. Elkeurti, A. Sayede, A. Tadjer, and F. Dahmane, J. Supercond. Novel Magn. **30**, 917 (2017).
28. K. Berriah, B. Doumi, A. Mokaddem, M. Elkeurti, A. Sayede, A. Tadjer, and J. P. Araujo, J. Comput. Electron. **17**, 909 (2018).
29. H. S. Saini, P. Mehra, S. Sinhmar, J. Thakur, and M. K. Kashyap, Vacuum **109760** (2020, in press). https://doi.org/10.1016/j.vacuum.2020.109760
30. P. Hohenberg and W. Kohn, Phys. Rev. B **136**, 864 (1964).
31. W. Kohn and L. J. Sham, Phys. Rev. A **140**, 1133 (1965).
32. P. Blaha, K. Schwarz, G. K. Madsen, D. Kvasnicka, and J. Luitz, in *WIEN2k, An Augmented Plane Wave + Local Orbitals Program for Calculating Crystal Properties,* Ed. by K. Schwarz (Tech. Univ. Wien, Wien, 2001).
33. D. J. Singh and L. Nordstrom, *Planewaves, Pseudopotentials, and the LAPW Method* (Springer Science, New York, 2006).
34. Z. Wu and R. E. Cohen, Phys. Rev. B **73**, 235116 (2006).
35. A. D. Becke and E. R. Johnson, J. Chem. Phys. **124**, 221101 (2006).
36. F. Tran and P. Blaha, Phys. Rev. Lett. **102**, 226401 (2009).
37. H. J. Monkhorst and J. D. Pack, Phys. Rev. B **13**, 5188 (1976).
38. F. Murnaghan, Proc. Natl. Acad. Sci. U. S. A. **30**, 244 (1944).
39. S. T. Weir, Y. K. Vohra, and A. L. Ruoff, Phys. Rev. B **33**, 4221 (1986).
40. M. Durandurdu, Chem. Phys. **367**, 80 (2010).

41. R. Bhattacharjee and S. Chattopadhyaya, J. Phys. Chem. Solids **110**, 15 (2017).
42. R. Bhattacharjee and S. Chattopadhyaya, Mater. Chem. Phys. **199**, 295 (2017).
43. S. Chattopadhyaya and R. Bhattacharjee, J. Alloys Compd. **694**, 1348 (2017).
44. B. Amimour, M. Slimani, C. Sifi, R. Khémissi, H. Meradji, S. Ghemid, S. B. Omran, and R. Khenata, Chin. J. Phys. **55**, 367 (2017).
45. J. P. Perdew and Y. Wang, Phys. Rev. B **45**, 13244 (1992).
46. J. P. Perdew, K. Burke, and M. Ernzerhof, Phys. Rev. Lett. **77**, 3865 (1996).
47. K. Yao, G. Gao, Z. Liu, and L. Zhu, Solid State Commun. **133**, 301 (2005).
48. G. Gao, K. Yao, E. ?cSaşıoğlu, L. Sandratskii, Z. Liu, and J. Jiang, Phys. Rev. B **75**, 174442 (2007).
49. R. J. Soulen, Jr., J. M. Byers, M. S. Osofsky, B. Nadgorny, T. Ambrose, S. F. Cheng, P. R. Broussard, C. T. Tanaka, J. Nowak, J. S. Moodera, A. Barry, and J. M. D. Coey, Science (Washington, DC, U. S.) **282**, 85 (1998).
50. K. Sato, H. Katayama-Yoshida, and P. Dederichs, J. Supercond. **16**, 31 (2003).
51. K. Sato, P. Dederichs, K. Araki, and H. Katayama-Yoshida, Phys. Status Solidi C **7**, 2855 (2003).
52. H. Akai, Phys. Rev. Lett. **81**, 3002 (1998).
53. S. Sanvito, P. Ordejon, and N. A. Hill, Phys. Rev. B **63**, 165206 (2001).
54. H. Raebiger, A. Ayuela, and R. Nieminen, J. Phys.: Condens. Matter **16**, L457 (2004).
55. C. Liu, E. Alves, A. Ramos, M. Da Silva, J. Soares, T. Matsutani, and M. Kiuchi, Nucl. Instrum. Methods Phys. Res., Sect. B **191**, 544 (2002).
56. B. Doumi, A. Tadjer, F. Dahmane, D. Mesri, and H. Aourag, J. Supercond. Novel Magn. **26**, 515 (2013).
57. Q. Mahmood, S. Ali, M. Hassan, and A. Laref, Mater. Chem. Phys. **211**, 428 (2018).